Phase Imaging by Atomic Force Microscopy: Analysis of Living Homoiothermic Vertebrate Cells

Eriko Nagao and James A. Dvorak
Laboratory of Parasitic Diseases, National Institute of Allergy and Infectious Diseases, National Institutes of Health, Bethesda, Maryland 20892-0425

ABSTRACT Atomic force microscope-based phase imaging in air is capable of elucidating variations in material properties such as adhesion, friction, and viscoelasticity. However, the interpretation of phase images of specimens in a fluid environment requires clarification. In this report, we systematically analyzed atomic force microscope-derived phase images of mica, glass, and collagen under the same conditions as used for living cells at various tapping forces; the resulting data provide critical information for the interpretation of phase images of living cells. The peripheral regions of COS-1 cells consistently show a more negative phase shift than the glass substrate in phase images at set-point amplitude: free amplitude (A_{sp}/A_0) = 0.6–0.8. In addition, at all A_{sp}/A_0 values suitable for phase imaging, tapping frequency appears to be high enough to ensure that phase shifts are governed primarily by stiffness. Consequently, phase imaging is capable of high resolution studies of the cellular surface by detecting localized variations in stiffness. We demonstrate that phase imaging of a bifurcating fiber in COS-1 cell cytoplasm is readily capable of a lateral resolution of ~30 nm.

INTRODUCTION

One mode of operation of the atomic force microscope (AFM) involves oscillating the cantilever at a high frequency. An advantage of this mode is that the probe makes only intermitted contact with the sample surface. Consequently, probe oscillations which are damped due to energy loss caused by the probe contacting the surface are gentler for the sample than conventional contact mode AFM where the probe is in continuous contact with the surface being scanned. Lateral and shear forces are reduced in tapping mode and changes in oscillation can be used to identify, map, and measure surface features. However, reports of tapping mode AFM imaging of living cells have been limited (Putman et al., 1994a,b; Vesenka et al., 1995; Schaus and Henderson, 1997). One reason might be that establishing proper AFM conditions, e.g., oscillation frequency, amplitude, set point, and scan rate, is more difficult when imaging living cells by AFM. We recently reported that tapping mode AFM could be used for long term, high resolution imaging of living cells (Nagao and Dvorak, 1998), and believe it may well become the principle technique for AFM studies of living homoiothermic vertebrate cells.

In phase imaging, a variant of tapping mode AFM imaging, the phase lag of the cantilever oscillation relative to the signal sent to the cantilever's piezo driver is used as a basis for image generation. Phase images can be generated as a consequence of variations in material properties such as adhesion, friction, and viscoelasticity (Babcock and Prater, 1995), and their interpretation in the material sciences is evolving rapidly (Magonov et al., 1997; Whangbo et al., 1997). However, the usefulness of phase imaging for biological materials has been explored only superficially (Hansma et al., 1997; Ohnesorge et al., 1997; Argaman et al., 1997).

In this report, we describe an analysis of phase images of living homoiothermic vertebrate cells immersed in fluid under highly controlled environment conditions together with studies of freshly cleaved mica, glass, and collagen samples imaged under identical conditions. We present height, amplitude, and phase AFM data at various A_{sp}/A_0 ratios, together with bright field light microscope (LM) images of the same sample. The vertebrate cell data were compared to and corrected with both mica and collagen data. Our studies result in an improved understanding of phase imaging in liquid of living cells, mica, and collagen and demonstrate a relationship to sample stiffness and/or viscoelasticity with minimal participation of adhesion forces.

MATERIALS AND METHODS

Sample preparation

We used COS-1 cells (ATCC CRL 1650), which were cultured and prepared for the AFM as described (Nagao and Dvorak, 1998). The mica (New York Mica Co., New York, NY) was freshly cleaved and mounted on a coverglass using a cyanoacrylate adhesive (Super Glue, GC Electronics, Rockford, IL). Collagen-coated coverglasses were prepared by covering a precleaned 25-mm diameter coverglass with a 200 μL drop of a 0.25 μg/μL collagen (Sigma Chemical Co., St. Louis, MO) solution in 0.1 N acetic acid. The coverglass was dried in a laminar flow tissue culture hood, and sterilized and cross-linked by UV irradiation overnight. The resulting coverglass was incubated in RPMI-1640 culture medium containing 5% fetal bovine serum (FBS) for at least 1 h to rehydrate the collagen. Using a 27 gauge, 0.5-inch hypodermic needle (Becton Dickinson, Rutherford,

Received for publication 21 May 1998 and in final form 31 March 1999.
Address reprint requests to James A. Dvorak, Ph.D., Laboratory of Parasitic Diseases, National Institute of Allergy and Infectious Diseases, National Institutes of Health, Building 4, Room 126, 4 Center Drive MSC 0425, Bethesda, MD 20892-0425. Tel: 301-496-4880; Fax: 301-480-1438; E-mail: jdvorak@atlas.niaid.nih.gov.

0006-3495/99/06/3289/09 $2.00

NJ), a cut was made through the center of the collagen layer and one-half of the collagen was peeled away exposing the glass surface. All samples were scanned at 32°C in RPMI-1640 or DMEM culture medium containing 5% FBS using a thermostated, controlled-environment culture system as described (Nagao and Dvorak, 1998).

AFM microscopy

We used a Bioscope AFM and a Nano-Scope III controller (Digital Instruments, Santa Barbara, CA). The Bioscope was mounted on an Axiovert 100 (Carl Zeiss, Thornwood, NY) inverted LM equipped with a Dimension AFM series G scanner head, quartz probe holder, rubber protective skirt, and a silicon nitride (Si_3N_4) probe (Model DNP, Digital Instruments, Santa Barbara, CA) with a 100 μm-long and 21 μm-wide V-shaped cantilever. The probes were treated with Sigmacote (Sigma Chemical Co., St. Louis, MO), which helps reduce the contamination of the probe tip (Nagao and Dvorak, 1998). The cantilever was tuned to resonate at 8.1–8.5 kHz in fluid and 46.0–47.0 kHz in air. A phase-extender module incorporating a lock-in amplifier (Digital Instruments, Santa Barbara, CA) was used to collect phase data. Phase imaging was performed at various tapping force ratios (i.e., 0.4–0.9; set-point amplitude (A_{sp}): free amplitude (A_0) as described by Magonov et al. (1997)). A constant set point was used for the serial scans, and changes in A_{sp}/A_0 were achieved by changing A_0 (65–147 nm). We established that $A_{sp}/A_0 = 0.4$ is the lowest value usable for imaging. All data were collected as 512×512 data arrays in the trace direction. Selected images were converted to ASCII format, and individual rows and/or columns were imported into Sigma Plot (SPSS Science, Chicago, IL) for analysis. None of the images in this report were subjected to signal processing.

Light microscopy

LM images were relayed into a chilled CCD video camera (model C5985, Hamamatsu Photonic Systems, Bridgewater, NJ), imprinted with a digital time stamp, and recorded continuously with a VHS video tape recorder (Model NV-8320, Panasonic, Secaucus, NJ). Individual LM images consisting of an average of 20 single-frame images were collected from video tape using a video frame grabber (Model 3155, Data Translation, Marlboro, MA) in a 266 MHz computer and averaged using the UTHSCSA Image Tool program, version 1.25 (University of Texas, San Antonio, TX) running under Microsoft Windows NT version 4.0.

RESULTS

Phase imaging of freshly cleaved mica

Freshly cleaved mica immersed in culture medium containing FBS displayed clearly observable steps or terraces of the mica layers by bright field LM (Fig. 1 *A*, *box*). AFM imaging was performed at A_{sp}/A_0 values of 0.4 to 0.9. Changes in the A_{sp}/A_0 ratio had no effect upon height images (Fig. 2 *A*, *left column*). In phase images, mica steps were also clearly demarcated in the $A_{sp}/A_0 = 0.5–0.9$ range. However, this demarcation disappeared at $A_{sp}/A_0 = 0.4$ (Fig. 2 *A*, *right column*). Height and phase shift differences between mica steps are plotted versus tapping force in Fig. 3 *A*. Height is nearly constant at all A_{sp}/A_0 values. Phase shifts show a similar pattern, except for $A_{sp}/A_0 = 0.9$. The values of height-dependent phase shifts were calculated at various tapping forces for each phase shift at each mica step height; the phase shift/100 nm height was nearly constant (Fig. 3 *B*). Maximal phase shift variations of 1 to 2° per 100 nm height occurred at $A_{sp}/A_0 = 0.5–0.8$. Visually, at $A_{sp}/A_0 = 0.5–0.9$, as the ratio decreased, the edges between terraces were enhanced, becoming darker and broader. However at $A_{sp}/A_0 = 0.4$, this edge effect disappeared. Freshly cleaved mica was also scanned in air using the same conditions as in fluid. Changes in the A_{sp}/A_0 ratio over a range of 0.4–0.9 had no effect upon either height images (Fig. 2 *B*, *left column*) or phase images (Fig. 2 *B*, *right column*).

Phase imaging of collagen immersed in culture medium

A bright field LM image showing the transition between the uncoated and collagen-coated regions of a coverglass is shown in Fig. 1 *B*. AFM height and phase imaging were performed over this transition region at A_{sp}/A_0 values of 0.4–0.9. Height images (Fig. 2 *C*, *left column*) confirm both

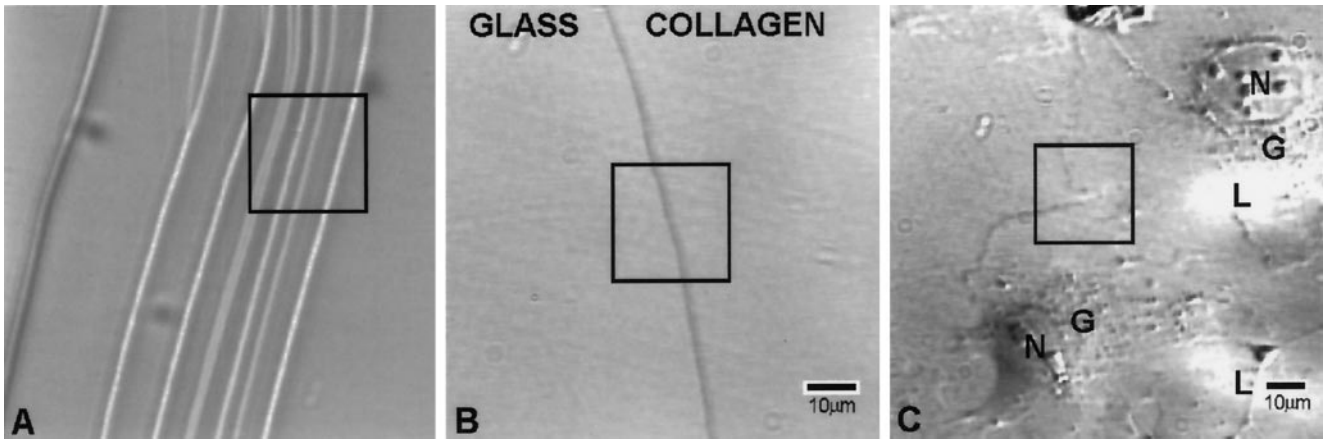

FIGURE 1 Bright field LM images of (*A*) freshly cleaved mica, (*B*) the interface between collagen and glass surfaces, and (*C*) COS-1 cells. The areas demarcated by the squares were imaged in the AFM. N, Nucleus; G, Golgi; L, laser beam. The bar represents 10 μm.

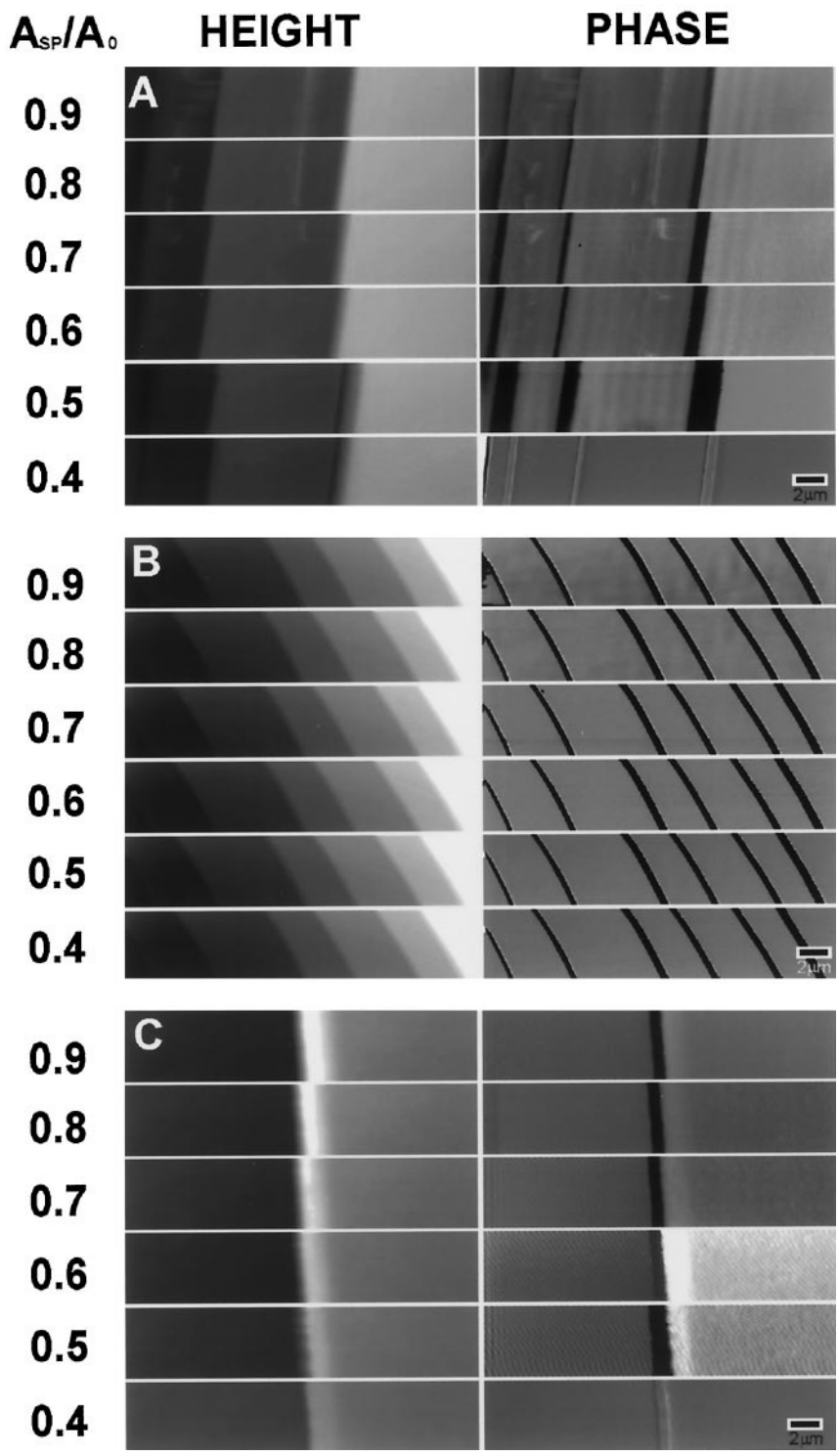

FIGURE 2 AFM images of a mica surface in fluid at various tapping forces (A_{sp}/A_0 = 0.4–0.9). (*A*) in fluid, (*B*) in air, and (*C*) a collagen-coated coverglass. Left and right columns show height and phase images, respectively. The bar (*lower right*) represents 2 μm.

the presence of collagen-free and collagen-containing regions of the glass surface and the uniformity of the collagen layer. A plot of collagen height versus tapping force is shown in Fig. 4 *A*. The apparent height of the collagen layer decreased gradually from 200 nm (A_{sp}/A_0 = 0.9) to 180 nm (A_{sp}/A_0, = 0.6); at A_{sp}/A_0 = 0.5 the apparent height decreased to 170 nm and at A_{sp}/A_0 = 0.4, decreased to 110 nm. When the A_{sp}/A_0 value was decreased gradually from 0.4 to 0.9 over a 30 min period, the apparent height of the collagen layer returned to 190 nm. Phase images (Fig. 2 *C*, *right column*) collected simultaneously with height images over the same A_{sp}/A_0 range displayed marked phase changes. These results, together with those of mica described above, imply that the collagen phase data also contain height information. Therefore, we averaged three phase shift/100 nm height values obtained from mica at

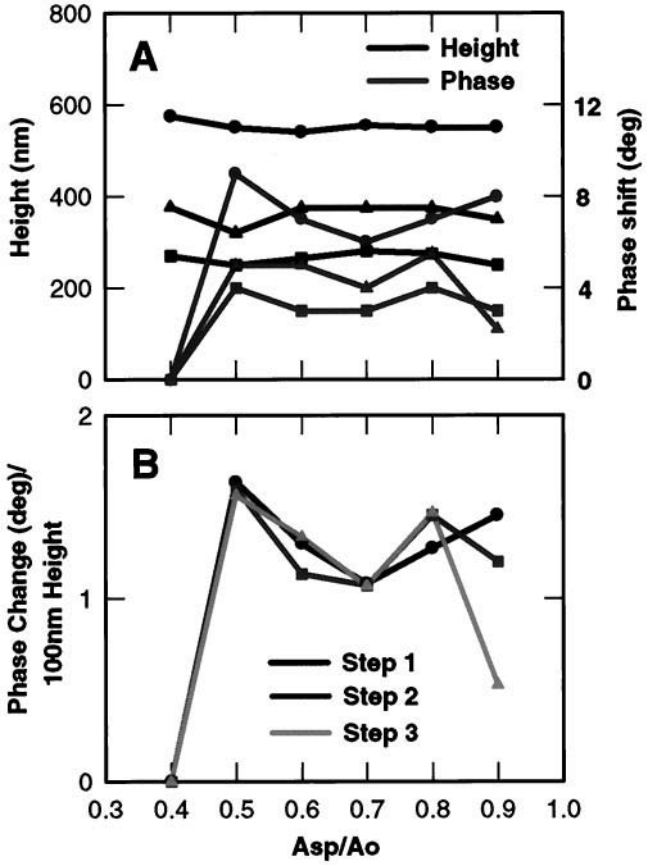

FIGURE 3 Graphical representation of height and phase changes for mica steps in fluid at various tapping forces (A_{sp}/A_0 = 0.4–0.9). (*A*) Height and phase differences for three steps were plotted versus tapping force. Step 1 (*circles*), step 2 (*squares*), and step 3 (*triangles*). (*B*) Phase shift values were normalized on the basis of height information present in each step. The resulting values were plotted versus tapping force. Symbols as in (*A*).

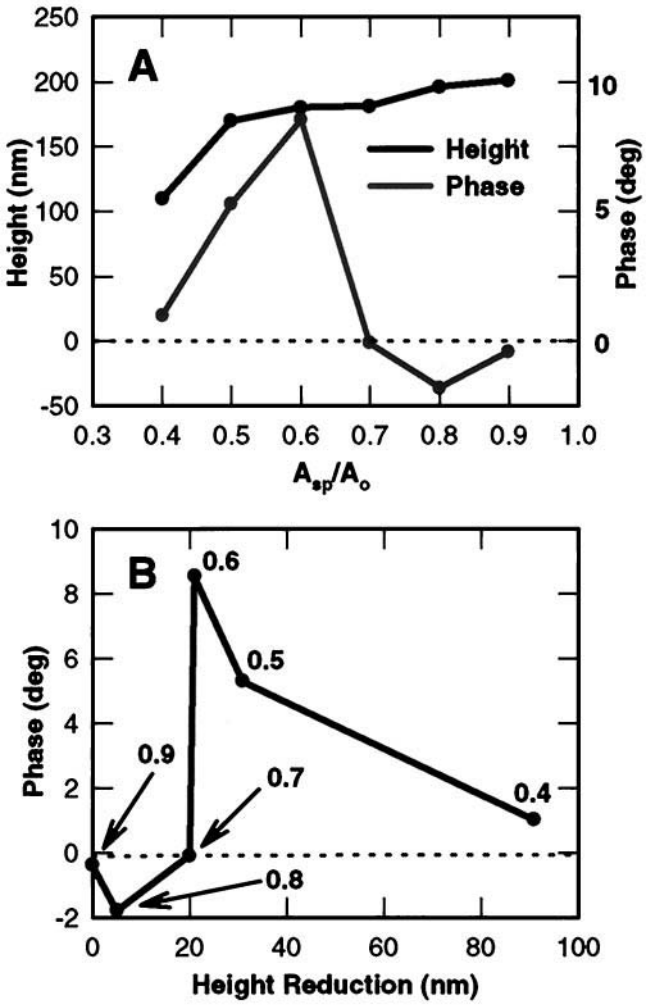

FIGURE 4 Graphical representation of height and phase changes for collagen in fluid at various tapping forces (A_{sp}/A_0 = 0.4–0.9). (*A*) Height (*black line*) and corrected phase (*gray line*) values were plotted versus tapping force. (*B*) Corrected phase values were plotted versus height reduction. The numbers on the graph represent the A_{sp}/A_0 values.

each tapping force and subtracted this height-induced phase shift artifact from the collagen phase shift data at the equivalent tapping forces. The corrected phase shift values were plotted versus both tapping force (Fig. 4 *A*, *gray line*) and height (Fig. 4 *B*). These plots show the contribution of the collagen layer relative to the coverglass substrate. Small negative phase shifts occurred at light tapping forces. At A_{sp}/A_0 = 0.5–0.6, there was a marked phase difference between the collagen and coverglass surfaces. A decrease in phase shift nearly proportional to the height of the collagen layer occurred at A_{sp}/A_0 = 0.4–0.5, whereas phase shift was independent of collagen height at A_{sp}/A_0 = 0.6–0.9. There was no detectable difference in phase images of adjoining coverglass and collagen surfaces at A_{sp}/A_0 = 0.4 (Fig. 2 *C*, *bottom right*) and the transition between the two surfaces is poorly demarcated as was the case with mica. However, a clear transition between these surfaces is present from A_{sp}/A_0 = 0.5–0.9, where the edge of the collagen is enhanced and becomes darker and broader as the A_{sp}/A_0 value decreases.

Phase imaging of living vertebrate cells

A bright field LM image of COS-1 cells is shown in Fig. 1 *C*. Nuclei and apparent Golgi regions in the cytoplasm are identifiable. Nucleolar structures are clearly visible in the nuclei. The laser beam is also shown as two out-of-focus bright spots at the sides of the AFM probe. AFM imaging was performed at A_{sp}/A_0 = 0.6–0.8 in the peripheral cytoplasmic region at the junction between two COS-1 cells. The cytoplasmic region of COS-1 cells, which is flat but very fragile, was chosen to minimize height-dependent phase shifts. Forces harder than A_{sp}/A_0 = 0.6 could not be used because they damaged the cells and induced rapid movement of the cytoplasm. Height, amplitude, and phase images at A_{sp}/A_0 = 0.6–0.8 are shown in Fig. 5. Although the height images (Fig. 5, *A*, *D*, and *G*) reveal surface topography, internal details such as lamellar and sparse fine fibrillar features are more clearly resolved in the amplitude images (Fig. 5, *B*, *E*, and *H*). The peripheral regions of

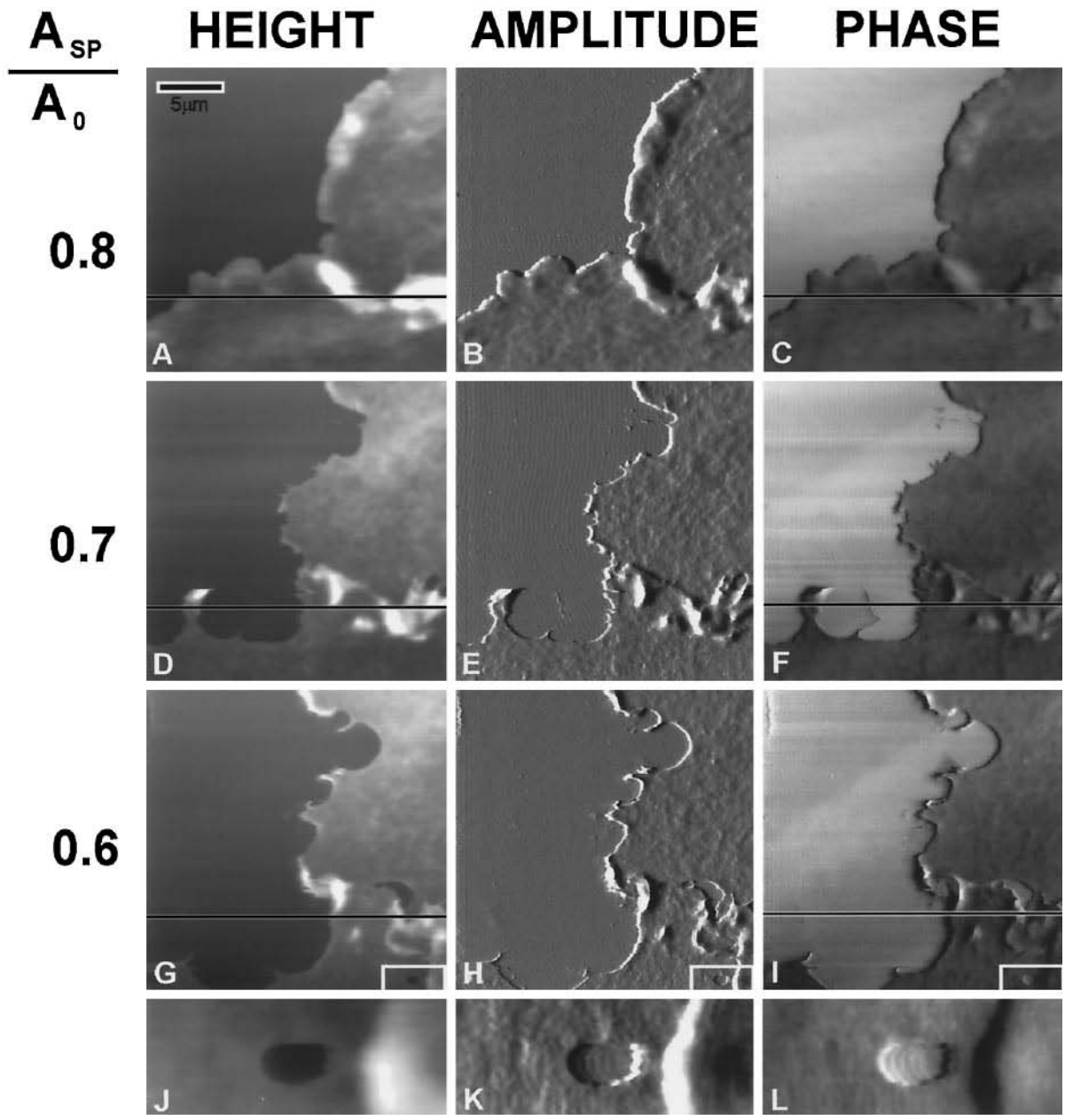

FIGURE 5 AFM images of the peripheral cytoplasmic region of COS-1 cells at various tapping forces ($A_{sp}/A_0 = 0.6–0.8$). (*A*) Height, (*B*) amplitude, and (*C*) phase images at $A_{sp}/A_0 = 0.8$; (*D*, *E*, *F*) at $A_{sp}/A_0 = 0.7$; and (*G*, *H*, *I*) at $A_{sp}/A_0 = 0.6$. (*J*, *K*, *L*), Enlarged height, amplitude, and phase images of the area demarcated by the rectangle in *G*, *H*, *I*. Cross-sections along the lines indicated in (*A*, *C*, *D*, *F*, *G*, *I*) are shown in Fig. 6. The bar (*upper left*) represents 5 μm.

COS-1 cells consistently show a more negative phase shift than the coverglass surface in phase images at $A_{sp}/A_0 = 0.6–0.8$ (Fig. 5, *C*, *F*, and *I*). As tapping force was increased from $A_{sp}/A_0 = 0.8$ to 0.6, the COS-1 cells were severely damaged by the AFM probe; at values below $A_{sp}/A_0 = 0.8$ (i.e., 0.7–0.6), COS-1 cell movement increased and the cells were damaged by the probe tip. However, probe-induced damage was not observed at tapping forces at or below $A_{sp}/A_0 = 0.8$ (i.e., 0.8–0.9). The area of the cell membrane demarcated by the rectangle in Fig. 5, *G*, *H*, and *I* is shown enlarged to 2×5 μm in Fig. 5, *J*, *K*, and *L*. Structural changes such as the appearance of a hole in the cytoplasm (Fig. 5, *J*, *K*, and *L*) appeared, cell locomotion increased, and the cell edges were degraded.

Cross-sectional traces of simultaneously acquired height and phase images at data row 128 from the bottom of the images are shown in Fig. 6 *A* and *B*, respectively. Neither the thickness (about 70 nm) nor the phase shift induced by the cytoplasm were influenced by modest tapping forces (i.e., $A_{sp}/A_0 = 0.6–0.8$). When phase data were corrected for height as described above, the COS-1 cells displayed a constant $-8°$ phase shift. However, as tapping force in-

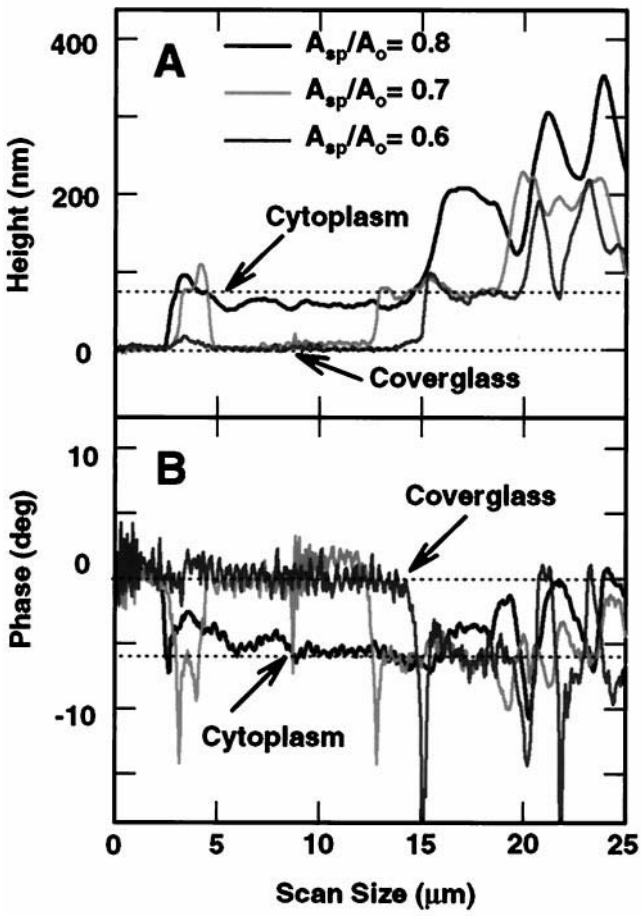

FIGURE 6 (*A*) Graphical representation of cross-sectional traces of height images at data row 128 from the bottom of the image as shown in Fig. 5, *A*, *D*, and *G* (*black*, *light gray*, and *dark gray lines*). The average height of the glass surface and the cytoplasmic peripheral region of COS-1 cells are represented by dotted lines. (*B*) Graphical representation of cross-sectional traces of phase images at data row 128 from the bottom of the image as shown in Fig. 5, *C*, *F*, and *I* (*black*, *light gray*, and *dark gray lines*). The average phase shift of the glass surface and the cytoplasmic peripheral region of COS-1 cells are represented by dotted lines.

creased, the edges of the cells exhibited increasingly negative phase shifts.

Serial images were collected at various magnifications in the cytoplasmic region of a COS-1 cell at $A_{sp}/A_0 = 0.8$ (Fig. 7). Although the cell moved slightly during the approximately 1-h course of data collection, the AFM images do not display any detectable deterioration in morphology at $A_{sp}/A_0 = 0.8$. The height images at all scan sizes (Fig. 7, *A*, *D*, and *G*) reveal both surface and subsurface details. However, at a scan size of 10 × 10 μm, features such as the numerous fibers criss-crossing the cell in various directions, are more clearly resolved in the amplitude image (Fig. 7 *B*) than in the height image (Fig. 7 *A*). At a scan size of 5 × 5 μm, the amplitude image (Fig. 7 *E*) loses definition and at 2.5 × 2.5 μm, the amplitude image (Fig. 7 *H*) is nearly featureless. In contrast, both surface and subsurface features are clearly resolvable in all 10 × 10 μm, 5 × 5 μm, and 2.5 × 2.5 μm phase images (Fig. 7, *C*, *F*, and *I*). A bifurcating fiber with a lateral resolution of 30 nm is discernible only in the phase image (Fig. 7 *I*, *arrow*).

Cross-sectional traces of height and phase images at data row 256 (of 512 rows) of the 100 μm^2, 25 μm^2, and 6.25 μm^2 scan areas depicted in Fig. 7 are shown in Fig. 8. The highest structural feature (Fig. 8 *A*, *arrow*) in the 100 μm^2 height image is less than 100 nm, and the corresponded phase feature shows a positive phase shift of about 3°. The magnitude of height variations in the 25 μm^2 (Fig. 8 *B*) and 6.25 μm^2 (Fig. 8 *C*) traces is within 50 nm and 40 nm, respectively, and the magnitude of the phase shift varies from +3 to +1.5°. Shoulders on peaks present in the height image trace are resolved as two peaks in the phase image trace (Fig. 8 *A*, *arrow*).

DISCUSSION

Variations in stiffness, adhesion, and viscoelasticity have all been postulated as factors affecting the observed differences in AFM-derived phase images. However, the interpretation of phase images, particularly of specimens immersed in fluid, requires clarification. For example, Argaman et al. (1997) imaged DNA molecules in aqueous buffers and concluded only that ". . . phase images often serve as a sort of 'second opinion' for height images." Consequently, we believe that a systematic analysis of AFM-derived phase images of control specimens such as mica, glass, and collagen in fluid at various tapping forces can provide critical information for the interpretation of phase images of biologically relevant molecules as well as living cells.

A mica surface was scanned at various tapping forces to elucidate effects of both height changes on phase images and the magnitude of the phase shift that occurs for a 100-nm height change. Babcock and Prater (1995) reported that phase imaging in air is not affected by large-scale height differences. However, we needed to confirm the generality of this phenomenon in both air and fluid before scanning living vertebrate cells, which generally have larger topographic changes than the materials used by Babcock and Prater (1995). Our results demonstrate that phase images of mica made in air at $A_{sp}/A_0 = 0.4–0.9$ do not include height information, even if there are larger topographic changes in the mica. In contrast, we also demonstrate that, with the exception of $A_{sp}/A_0 = 0.4$ when scanning is performed in fluid, height information is present to a variable degree in all phase images of mica. Although the height of the steps varies, the physical properties of each mica step are identical; a 1–2° phase shift/100 nm height occurred at all tapping force ratios except at $A_{sp}/A_0 = 0.4$. We do not have an exact physical explanation for this phenomena. We can only speculate that these phase differences in fluid might be caused by the effects of hydrodynamics and/or a lower oscillation frequency than in air. We have no data to confirm this speculation or support the premise that simply placing the scanner in fluid will change its linearity. These data imply that, if the height of a vertebrate cell is 3 μm, a

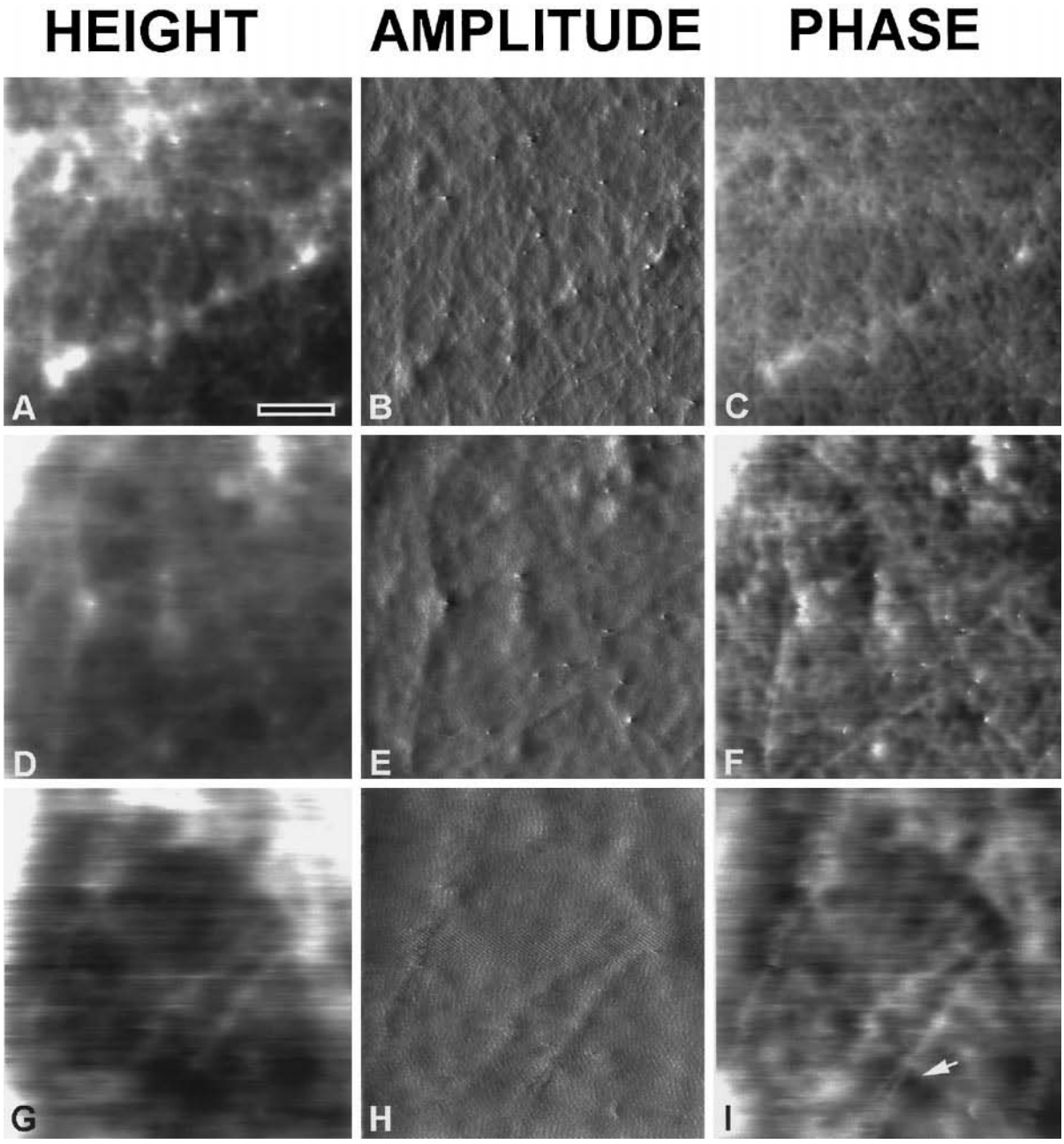

FIGURE 7 AFM images of the peripheral cytoplasmic region of COS-1 cells at $A_{sp}/A_0 = 0.8$. (*A*, *B*, *C*), Height, amplitude, and phase images at a scan size of 10 × 10 μm; (*D*, *E*, *F*) 5 × 5 μm; (*G*, *H*, *I*) 2.5 × 2.5 μm. The bifurcating fiber is indicated by the arrow in *I*. The bar (*upper left*) represents 2 μm in *A*, *B*, and *C*, 1 μm in *D*, *E*, and *F*, and 0.5 μm in *G*, *H*, and *I*.

height-dependent phase shift of 30–60° also may occur. Consequently, when phase imaging of living vertebrate cells is anticipated, a flat and thin region of the cytoplasm should be chosen, if possible. Furthermore, the phase image should be corrected by the removal of the height component obtained by imaging mica steps under identical conditions. This is important when the cell is scanned at tapping forces lower than $A_{sp}/A_0 = 0.4$.

We observed that, at various tapping forces, phase shift transitions in collagen are much different from those in vertebrate cells. It has been suggested that the major factors affecting phase shifts in soft materials are viscoelastic properties and adhesion forces with little participation by elastic properties (Tamayo and Garcia, 1996). In addition, it has been shown that, at light tapping forces and small A_0, tip-sample contact is minimal and the response of the cantilever is strongly influenced by surface forces such as capillarity and adhesion (Magonov et al., 1997; Whangbo et al., 1997). However, we believe that the influence of adhesive forces may be markedly reduced in fluid, especially in culture medium containing FBS, as a consequence of the interference of water and/or serum protein molecules. This

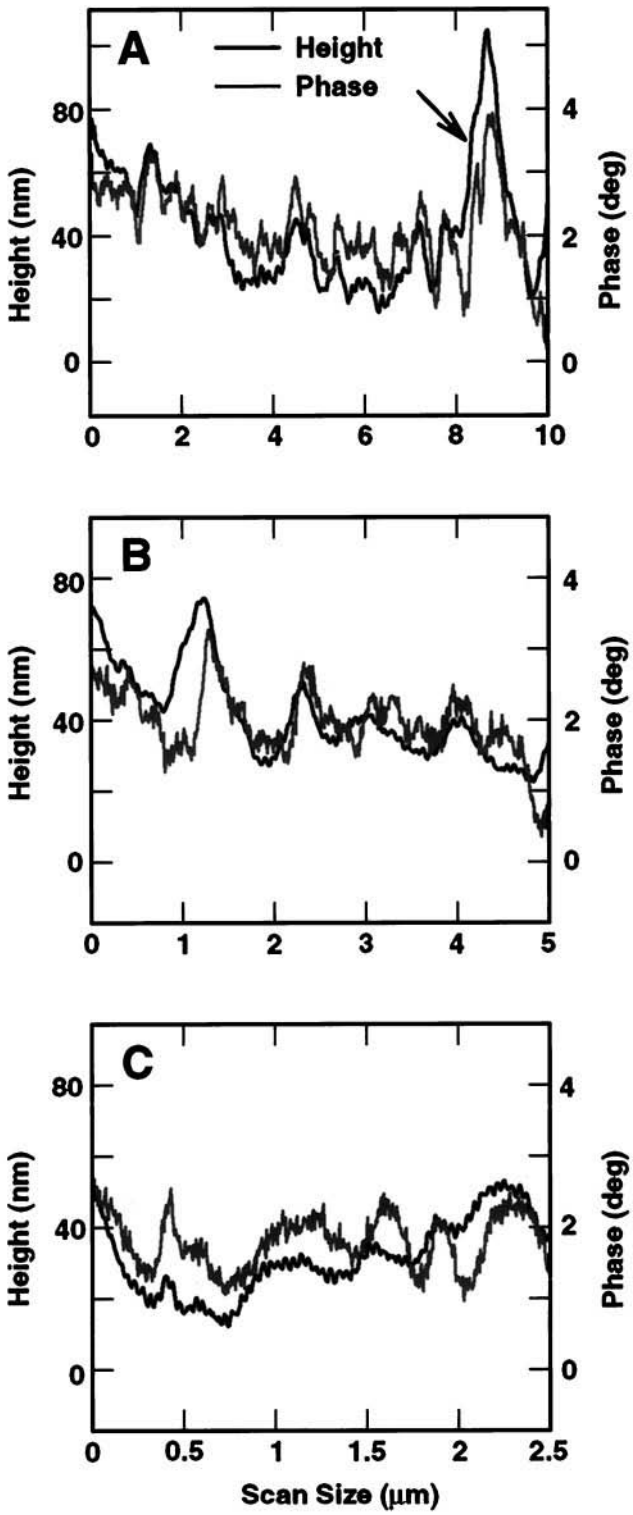

FIGURE 8 (*A*) Graphical representation of cross-sectional traces of height (*black line*) and phase (*gray line*) images at data row 256 as shown in Fig. 7, *A* and *C*; (*B*) in Fig. 7, *D* and *F*; and in (*C*) in Fig. 7, *G* and *I*. The arrow points out the shoulder of a peak in the height trace.

implies that intrinsic physical properties of samples may be detected in phase images collected in a fluid environment. This concept is supported further by the observation that, in vertebrate cells, phase shift transitions are not affected by changes in tapping force.

Phase imaging provides a map of stiffness variations on the sample surface; a stiffer region has a more positive phase shift than a less stiff region and, hence, appears brighter in a phase image (Magonov et al., 1997; Whangbo et al., 1997). Viscoelasticity is also a major factor affecting phase shifts of soft materials (Tamayo and Garcia, 1996). We hypothesize that there are two principle contributions to the phase shifts we found in our study. One contribution to phase shift is related to stiffness, whereas a second component is the result of viscoelasticity. Therefore, the phase shifts occurring in a fluid environment arise from a mixture of information from these two sources. Glass represents the hardest and stiffest surface imaged in our study. Theoretically, if we were to image structures that are harder or stiffer, they would exhibit a more positive phase shift relative to the glass. Conversely, structures softer and/or more viscoelastic would produce negative phase shifts relative to the coverglass. One of the problems involved in making a direct comparison between the objects we studied, however, is that all of the phase values are relative to the zero phase point established by the operator during changes in A_{sp}/A_0. Consequently, although we did observe phase shift changes in COS-1 cells, for example, which were of a lower magnitude (i.e., negative) relative to the coverglass substrate, we could not determine the absolute value of these phase shifts. In contrast, the phase shifts occurring in collagen and COS-1 cells are relatively lower than those of glass, implying that, in these softer materials exhibiting a negative phase shift, the viscoelastic component prevails. The seemingly anomalous positive shift observed in collagen at $A_{sp}/A_0 = 0.6$ may reflect a greater contribution of viscoelasticity than stiffness. The decrease in phase shift accompanied by a decrease in height at $A_{sp}/A_0 = 0.5$ may be the consequence of the reorientation of collagen molecules and the redistribution and/or the exclusion of water from the collagen layer (Mow et al., 1989). Both phenomena could cause a decrease in viscoelastic response and an increase in stiffness, reflecting a transition between these two properties.

The data of mica, collagen, and vertebrate cells demonstrate that the magnitude of the edge-enhancement effect also depends upon tapping force. Neither phase shift nor edge enhancement was detected in either a collagen-coated coverglass or a mica surface at $A_{sp}/A_0 = 0.4$. These data corroborate the reports of Magonov et al. (1997) and Whangbo et al. (1997) that the contrast of a phase image at moderate tapping forces ($A_{sp}/A_0 = 0.4–0.7$) is reversed at hard tapping forces ($A_{sp}/A_0 < 0.3$). The disappearance of a phase shift at $A_{sp}/A_0 = 0.4$ in our study further supports their observations. We propose that the A_{sp}/A_0 value of 0.4 may be the inflection point for contrast inversion of a phase image in fluid. Magonov et al. (1997) and Whangbo et al. (1997) concluded that, when imaging in air, a phase contrast reversal was the result of an increase in the effect of tip-sample contact area and contact time on stiffness as the A_{sp}/A_0 value was lowered. However, when imaging in fluid,

we do not believe that the disappearance of the positive shift in collagen can be explained by a change in tip-sample contact area or contact time. We believe another mechanism must be involved when imaging in fluid, because the contact area and stiffness over collagen should increase and present a more positive shift than the contact area and stiffness over glass at hard tapping forces. In addition, the disappearance of a phase shift in mica cannot be explained by a change in contact area.

The peripheral regions of COS-1 cells present phase shift transitions that are different from those of collagen. Whangbo et al. (1997) suggested that, when imaging in air, soft polymers would behave as elastic solids, and phase shifts would be governed by stiffness properties when the relaxation frequencies of viscoelastic polymers are significantly lower than the tapping frequencies used to collect the images. Putman et al. (1994a,b) found that the tapping frequencies used for imaging living cells are greater than the relaxation times due to the viscoelasticity of the cells. We observed that, in phase imaging of COS-1 cells, the tapping frequency appears to be high enough to ensure that phase shifts are governed primarily by stiffness. Our results in COS-1 cells fortify the proposition that phase imaging provides a map of stiffness variations on the COS-1 cell surface such that a stiffer region has a more positive phase shift and hence appears brighter in a phase image.

The peripheral region of COS-1 cells is more fragile and has a smaller elastic region in the stress–strain curve (Nordin and Frankel, 1989) than does collagen under identical scanning conditions. This interpretation is fortified by our observation of probe-induced hole formation in the cell cytoplasm at $A_{sp}/A_0 = 0.6$ without concomitant deformation. In the magnified images of the peripheral region of the cell, phase shift differences can be detected on the surface. However, the extent of the shift variations is much less than those occurring between the cell surface and the coverglass. Although height information should be present in the phase images of the cell surface, the relative relationship between height and phase shifts implies that phase shifts form the major contribution to surface images. If the residual height information is removed, a true phase image reflecting cell surface stiffness should result. Cytoplasmic areas containing internal fibers show more positive phase shifts than do areas where fibers are absent. These positive phase shifts are undoubtedly also the result of localized fiber stiffness. We demonstrate that phase imaging was capable of resolving subsurface fibers at a lateral resolution of ~30 nm.

In conclusion, phase imaging is capable of higher resolution imaging of the surface of living cells, demonstrating stiff subsurface structures and property changes resulting from changes in stress loading. These attributes imply that AFM-based phase imaging will be an important and useful tool in the medical, cell biological, and biomechanical fields.

We thank Dr. Sergei Magonov and Matt Thompson of Digital Instruments for helpful discussions during the course of this work and Carol C. Cunnick, Laboratory of Parasitic Diseases, NIAID, for technical assistance.

REFERENCES

Argaman, M., R. Golan, N. H. Thomson, and H. G. Hansma. 1997. Phase imaging of moving DNA molecules and DNA molecules replicated in the atomic force microscope. *Nucleic Acids Res.* 25:4379–4384.

Babcock, K. L., and C. B. Prater. 1995. Phase imaging: beyond topography. Application Note 11, Digital Instruments, Santa Barbara, CA.

Hansma, H. G., K. J. Kim, D. E. Laney, R. A. Garcia, M. Argaman, M. J. Allen, and S. M. Parsons. 1997. Properties of biomolecules measured from atomic force microscope images: a review. *J. Struct. Biol.* 119: 99–108.

Magonov, S. N., V. Elings, and M.-H. Whangbo. 1997. Phase imaging and stiffness in tapping-mode atomic force microscopy. *Sur. Sci. Lett.* 375: L385–L391.

Mow, V. C., C. S. Proctor, and M. A. Kelly. 1989. Biomechanics of articular cartilage. *In* Basic Biomechanics of the Musculoskeletal System. 2nd ed, M. Nordin and V. H. Frankel, editors. Lea and Febiger, London. 31–58.

Nagao, E., and J. A. Dvorak. 1998. An integrated approach to the study of living cells by atomic force microscopy. *J. Microscopy*. 191:8–19.

Nordin, M., and V. H. Frankel. 1989. Biomechanics of bone. *In* Basic Biomechanics of the Musculoskeletal System. 2nd ed, M. Nordin and V. H. Frankel, editors. Lea and Febiger, London. 3–29.

Ohnesorge, F. M., J. K. Horber, W. Haberle, C. P. Czerny, D. P. Smith, and G. Binnig. 1997. AFM review study on pox viruses and living cells. *Biophys. J.* 73:2183–2194.

Putman, C. A. J., K. O. Van der Werf, B. G. De Grooth, N. F. Van Hulst, and J. Greve. 1994a. Viscoelasticity of living cells allows high resolution imaging by tapping mode atomic force microscopy. *Biophys. J.* 67: 1749–1753.

Putman, C. A. J., K. O. Van der Werf, B. G. De Grooth, N. F. Van Hulst, and J. Greve. 1994b. Tapping mode atomic force microscopy in liquid. *Appl. Phys. Lett.* 64:2454–2456.

Schaus, S. S., and E. R. Henderson. 1997. Cell viability and probe-cell membrane interactions of XR1 glial cells imaged by atomic force microscopy. *Biophys. J.* 73:1205–1214.

Tamayo, J., and R. Garcia. 1996. Deformation, contact time, and phase contrast in tapping mode scanning force microscopy. *Langmuir*. 12: 4430–4435.

Vesenka, J., C. Moscher, S. Schaus, L. Ambrosio, and E. Henderson. 1995. Combining optical and atomic force microscopy for life sciences research. *BioTechniques*. 19:240–249.

Whangbo, M.-H., S. N. Magonov, and H. Bengel. 1997. Tip-sample force interactions and surface stiffness in scanning probe microscopy. *Probe Microsc.* 1:23–42.